

A Detection Method for Small Kuiper Belt Objects: The Search for Stellar Occultations

Françoise Roques and Michel Moncuquet

Département de Recherche Spatiale, Observatoire de Paris, 5, Place Jules Janssen, 92195 Meudon, France

E-mail: roques@obspm.fr

Received November 30, 1999; revised March 30, 2000

We explore the possibility of detecting small Kuiper belt objects (KBO) by serendipitous observation of stellar occultations: We show that such unpredictable occultations may allow us to detect a population of very small objects (typically of ~ 100 m radius at 40 AU), invisible by any other observational method, as long as (i) the assumed population fills up a sufficient area on the sky plane, (ii) the instrumental sensitivity and acquisition frequency are high enough, and (iii) the observed star has a small angular radius. This result is basically due to the diffractive broadening of the geometric shadow of small (assumed numerous) occulting objects. This diffractive broadening is more pronounced for smaller stellar disks and better photometric precision. Assuming there exist about 10^{11} objects of radius $\rho > 1$ km, located between 30 and 50 AU near the Ecliptic, and that the differential size distribution varies as ρ^{-q} with the index $q = 4$ extending down to decameter-sized objects, we expect a number of valid occultations (i.e., a 4σ event) between a few to several tens per night, if we may obtain an rms signal fluctuation $\sigma \lesssim 1\%$ and observe a star in the ecliptic with an angular radius $\lesssim 0.01$ mas. Since this occultation rate is very sensitive to the index slope q and plummets when $q \lesssim 3$, a KBO occultation observation campaign could provide a decisive constraint on the actual slope of the KBO size distribution for subkilometer-sized objects. Blue O class stars are the best candidates for detecting KBOs since they have the smallest angular radius for a given visual magnitude. The occultation events are typically very brief ($\lesssim 1$ s) and they are shorter but more numerous when observed in the antisolar direction, so rapid photometry (> 1 Hz) is required and high-speed photometry ($\gtrsim 20$ Hz) is preferred. The French space mission *Corot* will provide an excellent opportunity to observe occultations by KBOs using high precision photometry. © 2000 Academic Press

Key Words: Kuiper Belt objects; occultations; photometry.

1. INTRODUCTION

The existence of a residual protoplanetary disk beyond the Neptune orbit was speculated by Kuiper (Kuiper 1951). The recent discovery of hundreds of objects (Jewitt 1999), with radii from 50 to 200 km and located between 30 and 50 AU confirms the reality of the Kuiper hypothesis. A simple extrapolation of the observations allows us to predict the existence of 40,000 to 70,000 objects of more than 50 km radius in this region, and

the existence of 10^{11} objects of more than 1 km radius. The observations also suggest that the differential size distribution is a power law ρ^{-q} (where ρ is the KBO radius) with an index $q \approx 4$ (Luu and Jewitt 1998). This value is compatible with the guess that the Kuiper belt is the “reservoir” of short-period comets. The total mass of these Kuiper belt objects (called KBOs hereinafter) is estimated from 0.1 to 0.3 Earth mass (Jewitt and Luu 1995). Actually, the density of matter in the outer Solar System seems surprisingly low beyond Neptune, and the Kuiper disk could be much larger than the present observations suggest. If the Kuiper disk has a size distribution with such a constant index extending down to meter-sized objects, it would include a huge number of subkilometer-sized objects. However, a large collision rate could have destroyed the smaller objects. Anyway, knowledge of the small KBO population is a key point because it could contain most of the Kuiper disk mass. The search for small KBOs is also a way to constrain the spatial distribution of the KBOs. The radial and vertical extensions of the Kuiper belt are very poorly known, in particular the outer limit of the Kuiper belt. It could extend to the Oort cloud with decreasing density. Furthermore, the Kuiper belt could be similar to some circumstellar dust disks (as, for example, observed around HR4796 by Schneider *et al.* 1999) that have a typical size of 100 AU and could be the residue of planet formation.

More generally, the structure of the Kuiper belt, its size, thickness, mass, and momentum distribution are key tools in the pursuit of planet formation, because the Kuiper belt is the most primitive part of the Solar System since it was the outer part of the protoplanetary system: In the inner part of the disk, the planetesimals collided to create larger bodies. Beyond Neptune, reduced collision rate prevented planet formation. Since then, the Kuiper disk has suffered little evolution: Except for the inner boundary which is connected to a resonance with Neptune, the giant planets are too far away to perturb the disk as they do the asteroid belt. Mass and momentum distributions, important parameters for planet formation scenarios, are poorly known in the outer Solar System where the time scales of the formation of Uranus and Neptune are not yet well understood.

Stellar occultations are a powerful tool for exploring the outer Solar System: They have provided rich information on planetary

atmospheres and ring systems (Elliot and Olkin 1996, Sicardy *et al.* 1991). However, the observation of a stellar occultation by a given small object, such as a known comet or an asteroid, is quite difficult because the small angular size of the object prevents a precise prediction of the shadow path (cf. prediction of occultations by Pholus in Stone *et al.* 1999). The possibility of detecting small objects of the Solar System by stellar occultation was introduced by Bailey (1976) and Dyson (1992). More recently, Brown and Webster (1997) have proposed to use the Macho experiment for detecting stellar extinction by KBOs, but in these works, the diffraction effect during occultations has been neglected. We will show here that taking star light diffraction into account is a *sine qua non* condition for addressing and implementing such a detection method.

We thus explore here the possibility of detecting KBOs by a method of “serendipitous occultations” by taking into account the diffraction effect: In Section 2, we discuss and estimate the statistical rate of occultation by KBOs using geometrical optics only, that is, without taking into account diffraction effects. In Section 3 we present a theoretical model of diffracted lightcurves produced during stellar occultation, and we show that occultations could make it possible to detect rather distant and small objects. In Section 4, we then use this model to estimate a occultation rate by KBOs more realistic than that estimated in Section 2, and we give the probability of detecting occultations by KBOs within the present capabilities of existing instruments. Section 5 explores the possibility of better exploiting the diffraction phenomenon for optimizing the detection of KBOs, especially when using high-precision photometric instruments, and discusses other possible instrumental implementations of such a method. Finally, in Section 6 we discuss how to be assured that the observed dips on a lightcurve are due to occultation, and in particular, due to occultation by KBOs.

2. THE STATISTICAL RATE OF STELLAR OCCULTATION BY KBOs: A FIRST APPROACH

The occultation statistical rate is the probable number of occultations of a star detected during a given time interval. When an observer (on the Earth in most cases) crosses the shadow of a KBO cast by a star, the star light is not fully extinguished and the stellar flux oscillates: If these oscillations are detected, there is an occultation, and the whole region where these oscillations can be detected is called the diffraction shadow. Thus, the occultation rate is computed as the probability of intersection in the sky plane of the star disc with the KBO’s diffraction shadow.

If, at first, we ignore diffraction, the definition of an occultation event simplifies: there is an occultation when the observer crosses the geometric shadow of a KBO, and the star light is fully or partially extinguished, depending only on geometric parameters linked to the KBO and to the star. In addition, the detection of an occultation event depends on the conditions of the observation and in particular on the instrument used for recording the occultation. In the following discussion, we estimate this

“geometric” occultation rate by KBOs for a given star; we defer the possibility of modeling and exploiting the diffraction phenomenon to later sections.

We consider a population of KBOs moving with respect to a star in the sky plane. There is an occultation of the star by a KBO if the minimum distance between the two objects is smaller than the sum of their radii. We may then write the number of geometric occultations of a star with angular radius Φ_* and with an inclination i on the ecliptic plane, by KBOs of angular radius between φ and $\varphi + d\varphi$, observed during an interval Δt as

$$n_{\text{occ}}(\varphi) = 2\delta(\varphi, i)(\varphi + \Phi_*)v_o\Delta t, \quad (1)$$

where $\delta(\varphi, i)$ and v_o are the density and velocity, respectively, of KBOs in the sky plane.

The total number of occultations during Δt is then

$$N_{\text{occ}} = \int_{\varphi_{\text{lim}}}^{\varphi_{\text{max}}} n_{\text{occ}}(\varphi) d\varphi, \quad (2)$$

where φ_{max} is the maximum expected angular radius of KBOs (this value is not critical since we know that big KBOs are very rare; i.e., $\delta(\varphi, i)$ must be vanishingly small for large φ) and φ_{lim} is the angular radius of the smallest KBO detectable by occultation.

Let us now discuss the three main parameters governing this geometric occultation rate:

1. *The density of the KBOs* is poorly known: The high magnitude of these objects limits the size of the directly detectable objects to a few kilometers, but we assume that the Kuiper belt has a size distribution $\propto \rho^{-q}$ with a constant index q extending to meter-sized objects. The near-Earth asteroid (NEA) population (the only small body population in the Solar System known down to meter-sized objects) indeed has a size distribution with an index more or less constant to 5 m radius (Rabinowitz *et al.* 1994). We will return to the assumption of a constant index q in Section 4. In addition, the KBOs are assumed to follow an exponential distribution in inclination with an angular scale height H , and the spatial density of KBOs is also assumed to depend on the distance to the Sun, D , with the same law as the protoplanetary disk, i.e., as D^{-2} . If we assume N KBOs larger than 1 km exist, located between 30 and D_{max} AU, the previous assumptions lead to the following 2-D differential size distribution ν , which is the number of KBOs of radius (in kilometers) between ρ and $\rho + d\rho$, with inclination (in degrees) between i and $i + di$, and at an heliocentric distance (in AU and >30 AU) between D and $D + dD$:

$$\nu(\rho, i, D) = \frac{180N}{4\pi^2} \frac{D^{-2}}{(D_{\text{max}} - 30)} \frac{C(H)}{H} e^{-\frac{i}{H}} (q-1)\rho^{-q}, \quad (3)$$

with

$$C(H) = \frac{\pi[(180/\pi)^2 + H^2]}{180[180/\pi + He^{-90/H}]} \simeq 1 + \sin^2 H,$$

where H is expressed in degrees, and ν is given per astronomical unit and per steradian.

Recent observations allow us to estimate there are 10^{11} objects larger than 1 km, located between 30 and 50 AU (the practical limit of existing surveys), with a differential size distribution index $q \approx 4$, and a latitudinal scale height $H = 30^\circ$ (Jewitt 1999). Then, by substituting these values into Eq. (3) and by integrating in D between 30 and 50 AU, we obtain the following mean density of KBOs in the sky plane of angular radius between φ and $\varphi + d\varphi$ and with inclination between i and $i + di$

$$\delta(\varphi, i) = 3 \cdot 10^{-11} e^{\frac{-i}{30}} \varphi^{-4}, \quad (4)$$

where, for convenience, φ is expressed in mas ($=0.001''$) and δ is so given per mas^2 . Let us note that if we assume the KBO size distribution ranges from one meter to some hundreds of kilometers (that is, from about 3×10^{-5} to 10 mas at 40 AU), we can estimate an optical depth of the Kuiper belt in the ecliptic of $\tau_{\text{KB}} \approx \int_{3 \times 10^{-5}}^{10} \delta(\varphi, 0) \varphi^2 d\varphi \approx 10^{-6}$. We will show however in Section 4 that diffraction perturbs the stars light far away from the geometric disc, such that the proportion of the ecliptic sky perturbed by the Kuiper belt is much larger than that inferred by the optical depth τ_{KB} .

2. *The velocity of the KBOs in the sky plane*, v_o , is involved in both the number of occultations ($N_{\text{occ}} \propto v_o$) and the duration of the occultation ($dt_o \propto 1/v_o$): It is given as

$$v_o = v_E \left(\cos \omega - \sqrt{\frac{1}{D_{\text{AU}}}} \right), \quad (5)$$

where D_{AU} is the heliocentric distance of the KBOs in astronomical units, v_E is the Earth's orbital speed, and ω is the angle between the KBO and the anti-solar direction which is called "opposition" hereinafter.

Because v_o depends on the distance D of the occulting objects, so do the probability and the duration of the occultations. This property could allow the discrimination between an occultation by a KBO and an occultation by an asteroid or a comet (see Section 6). By fixing D to 40 AU and having $v_E \approx 30$ km/s, we get $v_o \approx 30(\cos \omega - 0.16)$ km/s ($\approx (\cos \omega - 0.16)$ mas/s). Then v_o is maximum (≈ 25 km/s) toward the opposition and decreases toward a direction, called the "quadrature" hereinafter, for which $\cos \omega \simeq 1/\sqrt{D_{\text{AU}}}$, i.e., $\pm 81^\circ$ for an object at 40 AU. An occultation, usually very brief, becomes slower in this direction. For instance, if an occultation by a 1-km radius KBO was detected, it could last from about 0.1 to a few seconds, as ω goes from the opposition to the quadrature.

3. *The size of the smallest KBOs detectable by occultation*, φ_{lim} , depends on the angular radius of the star Φ_\star and on that of the KBO itself: An object that is too small passing in front of the star will not generate a detectable decrease in the stellar flux. For a KBO smaller than the stellar disc, geometrical optics gives the straightforward condition

$$\left(\frac{\varphi}{\Phi_\star} \right)^2 \geq \epsilon, \quad (6)$$

where ϵ is the detection threshold or sensitivity of the instrument. This yields, for instance, a detection threshold $\varphi_{\text{lim}} = 2 \cdot \Phi_\star \sqrt{\sigma}$ at $\epsilon = 4\sigma$, where σ is the rms signal fluctuations (i.e., the photometric precision limit of the instrument), with Φ_\star typically about 0.01 to 1 mas. However, as we shall see in subsequent sections, these formulas are quite approximate and only valid for a large stellar radius (>0.1 mas) because diffraction is not taken into account: the real detection threshold not only depends on the star size in a very different way than stated here, but it also depends on both the distance from the KBO to the observer and the observation wavelength.

We may finally deduce from Eqs. (2) and (4) and the discussion above the following approximation of the total number of geometric occultations by KBOs of a star with an angular radius Φ_\star and an inclination i on the ecliptic

$$N_{\text{occ}}(\Phi_\star, i) \approx 2 \cdot 10^{-7} v_o \Delta t e^{\frac{-i}{30}} \int_{\varphi_{\text{lim}}}^{10 \text{ mas}} \varphi^{-4} (\varphi + \Phi_\star) d\varphi, \quad (7)$$

where v_o is expressed in mas per second, Δt in hours, and φ_{lim} and Φ_\star in mas. For instance, we may estimate the geometric occultation rate per night (8 h) in the ecliptic for a $\epsilon = 4\sigma$ sensitivity and $\Phi_\star > 0.1$ mas as

$$N_{\text{occ}}(\Phi_\star, 0) \approx 1.5 \cdot 10^{-7} v_o \Phi_\star^{-2} \sigma^{-1.4}. \quad (8)$$

So this geometric occultation rate per night is less than 0.1 in the most favorable case, with a typical KBO detection threshold of a few kilometers in size. Fortunately, as we will show in Section 4, this result, which does not take into account any diffraction effects, significantly underestimates N_{occ} .

3. MODELING A REALISTIC STELLAR OCCULTATION BY A KBO

3.1. Basics

The light emitted by a point source (assumed to be at infinity to yield planar waves) incident on a sharp-edged obstacle (such as a KBO) is diffracted. Owing to the Huygens–Fresnel principle of wave propagation, each point of a wave front may be considered as the center of a secondary disturbance giving rise to spherical wavelets, which mutually interfere. If part of the original wave front is blocked by an obstacle, the system of secondary waves is incomplete, such that diffraction occurs. When observed at a finite distance D from the obstacle, this effect is known as "Fresnel diffraction," and falls within the scope of the Kirchhoff diffraction theory, which remains valid as long as the dimensions of the diffracting obstacles are large compared to the observed wavelength λ and small compared to D (cf. Born and Wolf 1980). The characteristic scale of the Fresnel diffraction effect (that is, roughly speaking, the broadening of the object shadow) is the so-called Fresnel scale $\sqrt{\lambda D/2}$. The Fresnel scale at 40 AU, observed at $\lambda = 0.4 \mu\text{m}$, is 1.1 km, i.e., a KBO typical size, and

so the diffraction must be seriously taken into account to analyze the occultations by KBOs.

Let us now consider the case of a monochromatic point source occulted by an opaque spherical object of radius ρ . If r denotes the distance between the line of sight (the star's direction) and the center of the object, and if the lengths ρ and r are expressed in the Fresnel scale unit (noted F_{su} hereinafter), the normalized light intensity $I_{\rho}(r)$ is given by (see Appendix B of Roques *et al.* 1987), outside the geometric shadow ($r \geq \rho$),

$$I_{\rho}(r) = 1 + U_1^2(\rho, r) + U_2^2(\rho, r) - 2U_1(\rho, r) \sin \frac{\pi}{2}(r^2 + \rho^2) + 2U_2(\rho, r) \cos \frac{\pi}{2}(r^2 + \rho^2), \quad (9)$$

inside the geometric shadow ($r \leq \rho$),

$$I_{\rho}(r) = U_0^2(r, \rho) + U_1^2(r, \rho), \quad (10)$$

where U_0 , U_1 , and U_2 are the Lommel functions defined by (for $x \leq y$)

$$U_n(x, y) = \sum_{k=0}^{\infty} -1^k (x/y)^{n+2k} J_{n+2k}(\pi xy), \quad (11)$$

where J_n is the Bessel function of order n .

Figure 1 (top) shows the diffraction pattern of a circular object (1 km radius) occulting a point star and is computed using Eqs. (9) and (10). The Fresnel scale is set to 1 km. The size of the shadow is larger (about one Fresnel scale) than the geometric shadow, and overall the diffraction fringes are visible at a large distance from the object (as long as the photometric sensitivity is good).

3.2. Discussion

Our aim is to compute a rate of occultations by KBOs more realistic (or a more confident threshold of KBO detection) than that computed in Section 2. Two points were not very realistic in the previous model of diffraction by a KBO: we have assumed (i) a perfectly circular object and (ii) the star is a point source. We thus discuss the following two provisos:

What about an irregularly shaped object? Of course, we do not expect to deal with perfect spherical objects in the Kuiper belt, while we need to model a random occultation with an isotropic diffraction pattern (i.e., which does not show preference to any direction in the observation plane). It is thus important to estimate the effects of an irregularly shaped object on the diffraction pattern. This study has been made by Roques *et al.* (1987) and the Fig. 1 (bottom) shows the diffraction pattern produced by an elliptical object ($e = 0.7$ and with similar size to the circular case, see legend) occulting a point star, computed from the code defined in that paper. To generate an extreme case, which could *a priori* smooth the diffraction fringes, the limb of the object has been corrugated by setting the ‘‘irregularity’’ parameter n to 3 (for its definition see Roques *et al.* 1987), that is,

an object about 6% hilly. Along the two axes of the ellipsoid, the diffraction fringes look like those of the circular object, while their structures are more complicated outwardly. However, if we compare the projected contours of the top and bottom of Fig. 1, one can see that these fringes are detectable, for a given sensitivity threshold (4% here), at distances larger or roughly equal to the distances where the fringes of the circular object are detected. We think therefore that using a circular object to compute the occultation lightcurve is a good ‘‘working compromise’’ for modeling an occultation by a realistic KBO.

Smoothing the occultation lightcurve on the star disk. We discuss here the fact that the occulted star is never a point source. Indeed, the apparent radius of a star projected at 40 AU could range from a fraction of a kilometer to several tens of kilometers (see Section 5), i.e., on the same order of magnitude as the KBOs. Therefore, the lightcurve smoothing over the apparent stellar disk must be taken into account in our computation. In order to do so, the star is considered as a set of incoherent point sources, with polar coordinates (s, θ) in a frame centered on the stellar disk. If r is now the distance in the occulting object plane from the star disk center to the object center, the normalized light intensity produced during an occultation of a stellar disk of apparent radius R_{\star} (again expressed in Fresnel scale units) becomes

$$I_{\rho}^{\star}(r) = \frac{2}{\pi R_{\star}^2} \int_0^{R_{\star}} s ds \int_0^{\pi} I_{\rho}(\sqrt{r^2 + s^2 + 2rs \cos \theta}) d\theta. \quad (12)$$

In Fig. 2 we present occultation lightcurves computed with Eq. (12) and produced by a 200-m (top) or a 1-km (bottom) KBO radius (within the two cases, a Fresnel scale of 1 km), for several different apparent stellar radii. As expected, the diffraction fringes are strongly smoothed when the apparent stellar size is larger than the KBO itself. An apparent stellar size of 2 km reduces the largest diffraction effect of a 200-m (1-km) occulting KBO to only about 2% (30%) of the star light instead of more than 10% (90%) with a small apparent stellar disk or a point source. The diffraction with a 10-km apparent star disk is no longer perceptible in this figure (though there is a 1% decrease in the light intensity for the 1-km object, which is simply the ratio of the areas, i.e., as the object transits the star disk).

3.3. What Could Be Finally Detected Thanks to Diffraction?

From the previous discussion, it appears that the diffraction effect during a stellar occultation by a KBO (and more generally by any small object in the Solar System) will depend as usual on its size and on the apparent distance from the star to the object (the impact parameter), but also strongly on the apparent stellar radius and on the Fresnel scale—that means, (i) that the star has to be well selected to optimize its apparent size and flux at the observed wavelength λ , and (ii) that such observations will generally need another means of estimating the distance D of the occulting object we are dealing with. We will return later to these two points, but if we assume these observational

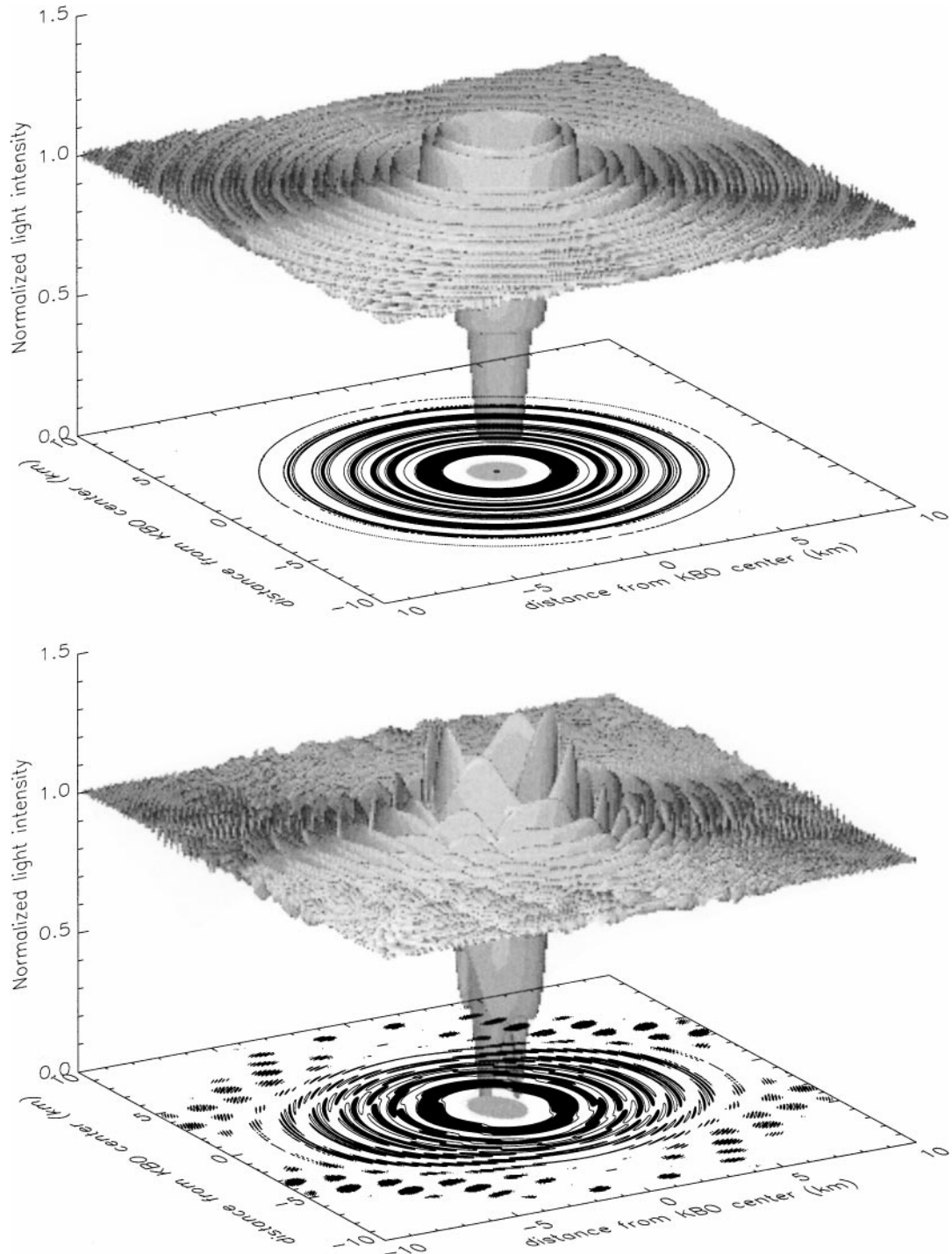


FIG. 1. The shadow pattern of a 1-km radius KBO in front of a point star. The two horizontal axis are distances in kilometers and the vertical axis is the normalized stellar flux. (Top) The KBO is circular. (Bottom) The KBO is irregular (the limb is $\sim 6\%$ corrugated) and elliptical (the eccentricity is 0.7 and the half major axis is $\frac{4}{3}$ km, such that $\frac{2}{3} < \rho < \frac{4}{3}$ km). The projected contours show the $\pm 4\%$ variation of the light intensity (the black filled areas correspond to $+4\%$, i.e., $I > 1.04$). The gray central spot indicates the exact geometric shadow of the KBO.

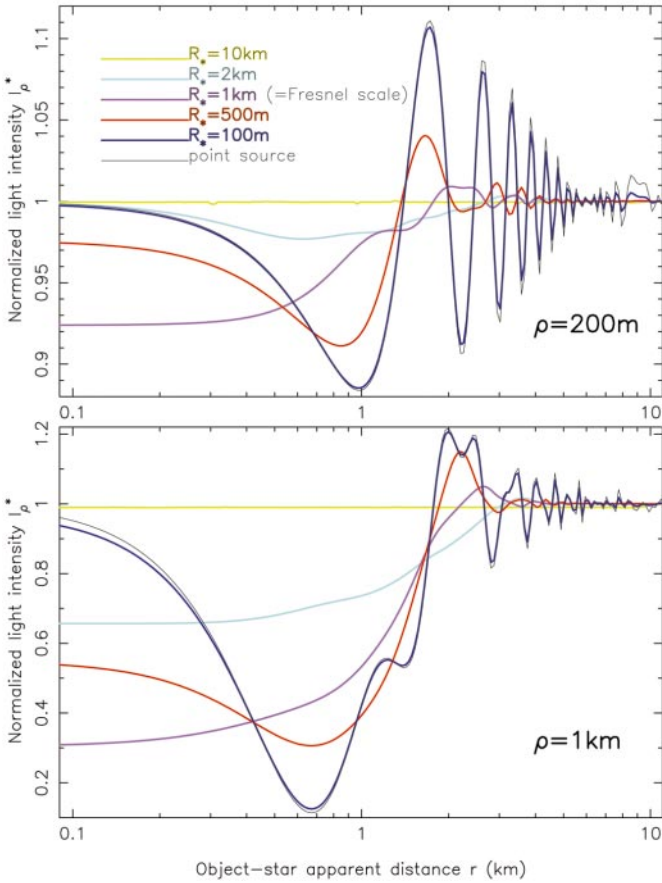


FIG. 2. Occultation profiles of a 200-m radius KBO (top) and a 1-km radius KBO (bottom), smoothed on different sized stars, for a 1-km Fresnel scale. The apparent stellar radii are 0 (thin black curve), 100 m (dark blue), 500 m (red), 1 km (purple), 2 km (cyan), 10 km (yellow).

parameters have been fixed, the ability to detect or not detect an object of a given size will then only depend on the photometric precision of the instrument.

To show this dependence in the most general way possible, Figs. 3a to 3e give the isolevels of fluctuation, that is, the maximum amplitude of the fluctuation of the stellar intensity, as a function of the real radius of the object and of the distance from the star to its center, both expressed in Fsu (and both on logarithmic scale). Each figure corresponds to a given apparent stellar radius (i.e., when projected in the occulting object plane) R_* , which is 1/10, 1/2, 1, 2, and 10 Fsu, respectively. On each figure, the gray zones correspond to the geometric shadow: the dark gray is the complete occultation zone and the light gray is the partial occultation zone.

Using Figs. 3a–3e, we may now define the diffraction shadow for a given sensitivity ϵ as the region where the diffraction fringes can be detected: $\rho_\epsilon(\rho, R_*)$ will denote the radius of the diffraction shadow of a given object (called “diffraction radius” hereinafter), which can be seen as the “occultation effective radius” of the object for a given star and a given photometric sensitivity. That is, on each figure, the isocontour of level ϵ simply yields

the diffraction radius ρ_ϵ as a function of the real radius object ρ . Finally, let us note that Figs. 3a–3e also yield the smallest detectable object ρ_{lim} for a given star radius R_* and a given sensitivity ϵ : it is the minimum reached by an isocontour of level ϵ .

Two points must be outlined from Figs. 3a–3e since they will have important consequences on the KBOs occultation rate computation, and more generally on photometric observations of stars in the ecliptic:

1. The diffraction shadow is generally much larger than the geometric shadow, and this “shadow broadening” is more pronounced as the apparent stellar disk size decreases and the photometric sensitivity increases. Moreover, one can see in Figs. 3a–3e that the broadening due to diffraction is about a factor 1000 around or slightly below the $\epsilon = 10^{-4}$ isocontour: that means, by comparison with the 10^{-6} KB optical depth estimated in Section 2 (assuming a density given by Eq. (4)), all the stars of the ecliptic could have their light perturbed at an amplitude level within the range $\sim [10^{-5}, 10^{-4}]$. Although such a fluctuation level is on the order of those due to star seismic pulsations, it should not perturb the seismological observations: each occultation event is brief (typically less than 1 s), such that it involves frequencies $\gtrsim 1$ Hz, compared to frequencies of 1 mHz and below typical of asteroseismology.

2. The apparent stellar radius, R_* , is a critical parameter, essentially because the occultation lightcurve is smoothed on the stellar disk, and this smoothing effect drastically increases the size of the smallest detectable objects (see Table I), while it generally reduces the diffraction radius: For a 1-Fsu object radius and a 10^{-3} photometric sensitivity, $\rho_{10^{-3}} \simeq 18$ Fsu for a quasi-point star, $\rho_{10^{-3}} \simeq 7$ Fsu for a 1-Fsu star apparent radius, and $\rho_{10^{-3}} \simeq 10$ Fsu for a 10-Fsu star, since in this case, the light fluctuation reduces $(\rho/R_*)^2$ (as in Eq. (6)) due to the simple transit of the object over the stellar disk (that is, the geometric partial occultation of the star).

4. THE STATISTICAL RATE OF A REALISTIC OCCULTATION BY KBOs

In Section 2, we defined the statistical rate of occultation as the probability of intersection in the sky plane of the star disc with the KBO’s diffraction shadow. The diffraction shadow, for a given sensitivity ϵ , has been defined in the previous section as the disk of radius $\rho_\epsilon(\rho, R_*)$, and given graphically (in Fsu) for some R_* . Therefore, the computation of the statistical rate of occultation remains basically the same as that in Section 2 except that:

- (i) We must express the differential size distribution ν given by Eq. (3) per squared Fresnel scale unit (instead of steradian). Then, by integrating ν in D between 30 and 50 AU, we obtain the mean KBO density per square kilometer:

$$\delta(\rho, i) = 1.4 \cdot 10^{-8} \frac{(1 + \sin^2 H)}{H} e^{-\frac{i}{H}} (q - 1) \rho^{-q}, \quad (13)$$

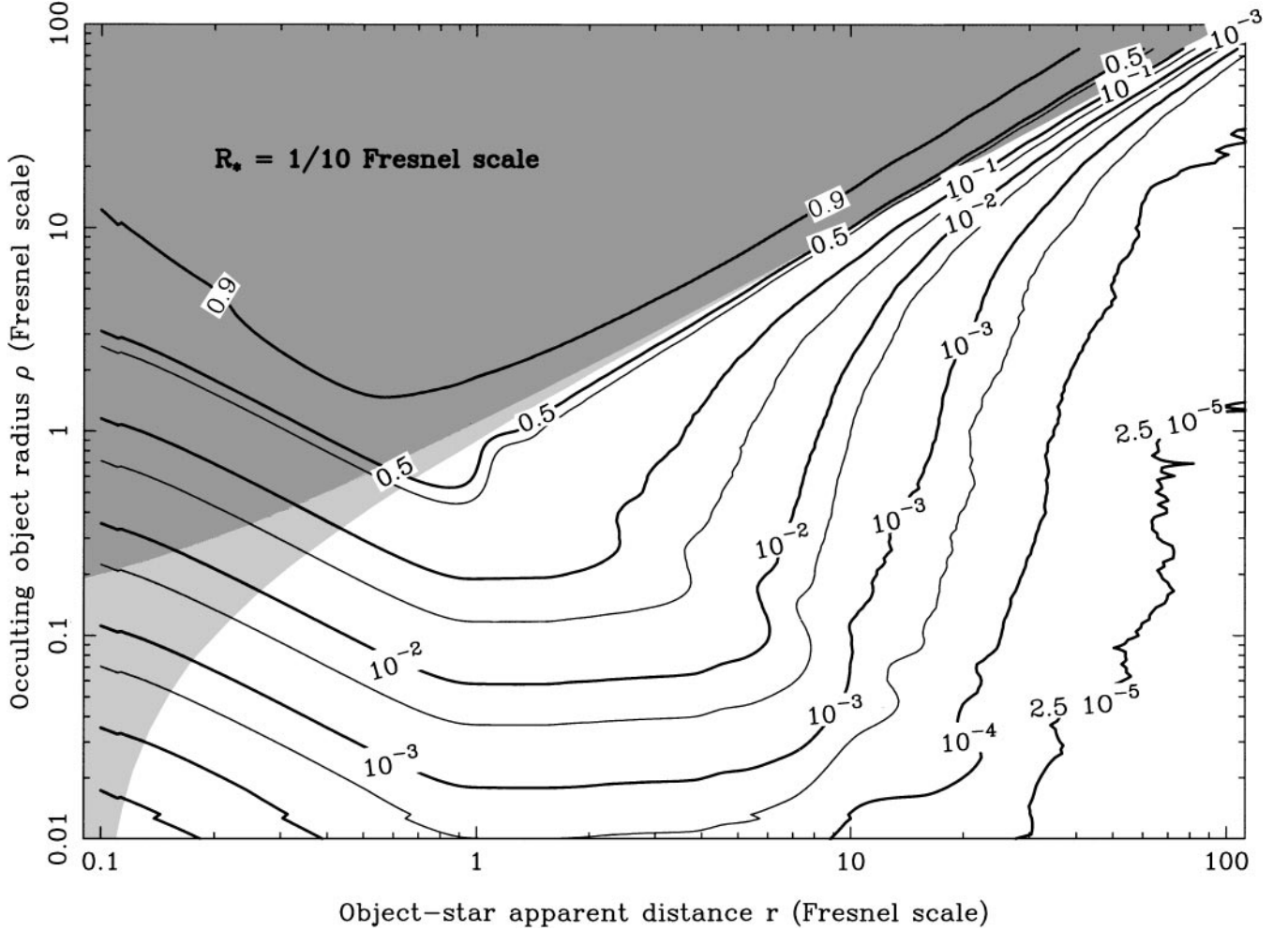


FIG. 3. Isocontours of the maximum amplitude variation of the normalized flux of a star occulted by an object, as a function of the distance from the line of sight to the KBO center (horizontal axis) and of the real object radius (vertical axis). The four nonlabeled thin contours are the ϵ isolevels for $\epsilon = 4 \times 10^{-4}, -3, -2, -1$. The gray zones correspond to the solution from geometric optics: the dark zone corresponds to a complete occultation and the light gray to a partial occultation. The figures were computed with different star sizes, namely with an apparent star radius of (a) $\frac{1}{10}\sqrt{\lambda D}/2$, (b) $\frac{1}{2}\sqrt{\lambda D}/2$, (c) $\sqrt{\lambda D}/2$, (d) $2\sqrt{\lambda D}/2$, and (e) $10\sqrt{\lambda D}/2$.

where ρ is expressed in kilometers, and i and H are expressed in degrees.

(ii) We must substitute the term into Eq. (1) taking into account the geometric partial occultation radius ($\varphi + \Phi_*$) by the diffraction radius $\rho_\epsilon(\rho, R_*)$, all expressed in Fresnel scale units.

We finally obtain an occultation statistical rate as

$$N_{\text{occ}}(R_*, i) \approx 10^{-4} v_o \Delta t (\sqrt{\lambda D}/2)^{2-q} \frac{(1 + \sin^2 H)}{H} e^{-\frac{i}{H}(q-1)} \times \int_{\rho_{\text{lim}}}^{200} \rho^{-q} \rho_\epsilon(\rho, R_*) d\rho, \quad (14)$$

where v_o is expressed in kilometers per second, Δt in hours, λ and D in kilometers, and all other distances in Fresnel scale units. Then $N_{\text{occ}}(R_*, i)$ needs to be numerically estimated using the graphical values of $\rho_\epsilon(\rho, R_*)$ and ρ_{lim} given by Figs. 3a–

3e: Some numerical results are summarized in Table I, which gives the occultation rate per 8 h observation in the ecliptic and the radius of the smaller detectable KBOs as a function of the stellar radius and the rms signal fluctuation σ (with a detection threshold $\epsilon = 4\sigma$), for a power law index of the size distribution $q = 4$. For comparison with the purely geometric rate given by Eq. (8), N_{occ} now varies roughly as σ^{-2} (for approximate stellar radii $\Phi_* < 0.01$ mas), while Eqs. (8) and (14) yield roughly the same rate for the largest stars.

The most important result from Table I is that the number of occultations for a star in the ecliptic could range from a few to several tens per night if we have good enough photometric precision (i.e., $< 1\%$) and a sufficiently small star (i.e., < 0.01 mas). This result is basically due to the diffraction broadening of small (assumed numerous) Kuiper belt objects.

Nevertheless, we must keep in mind the assumptions concerning the population of KBOs which lead to the numbers of Table I:

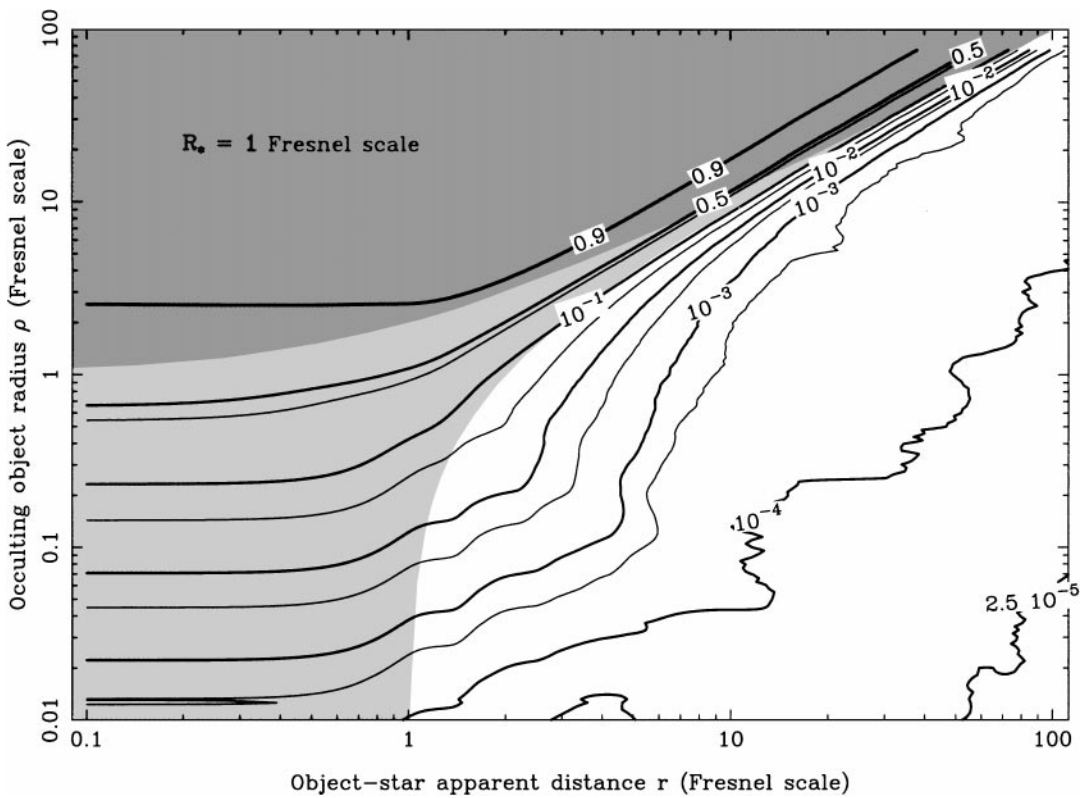
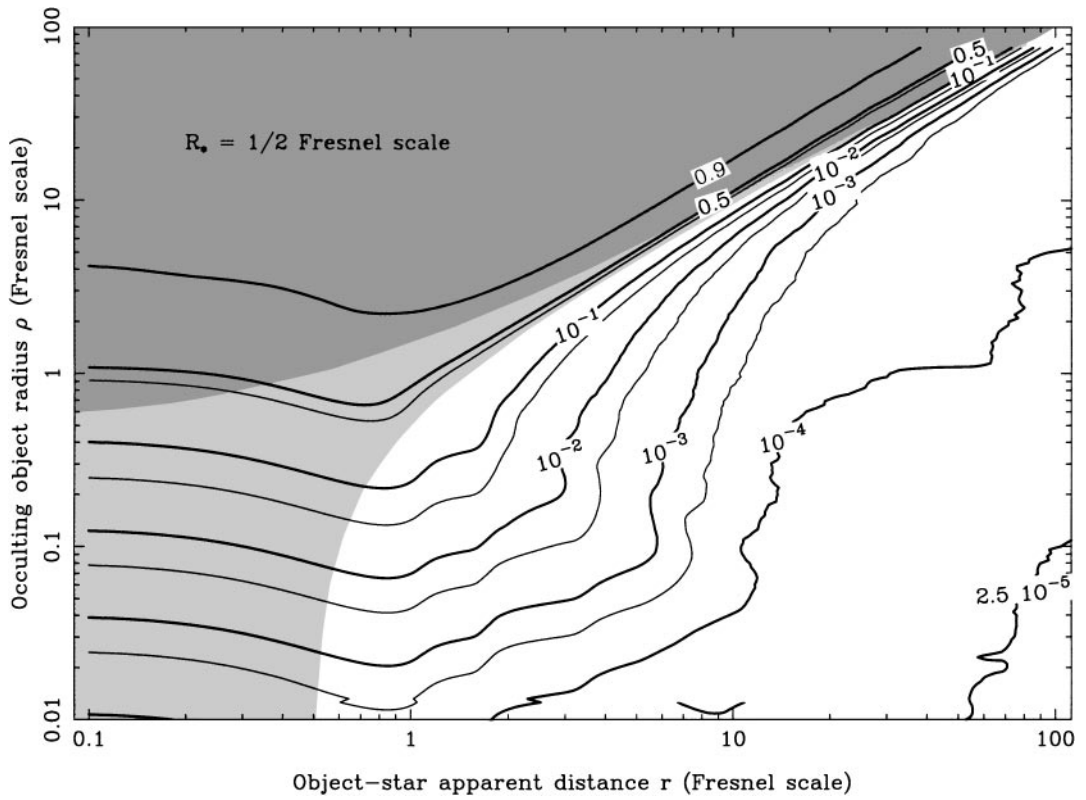


FIG. 3—Continued

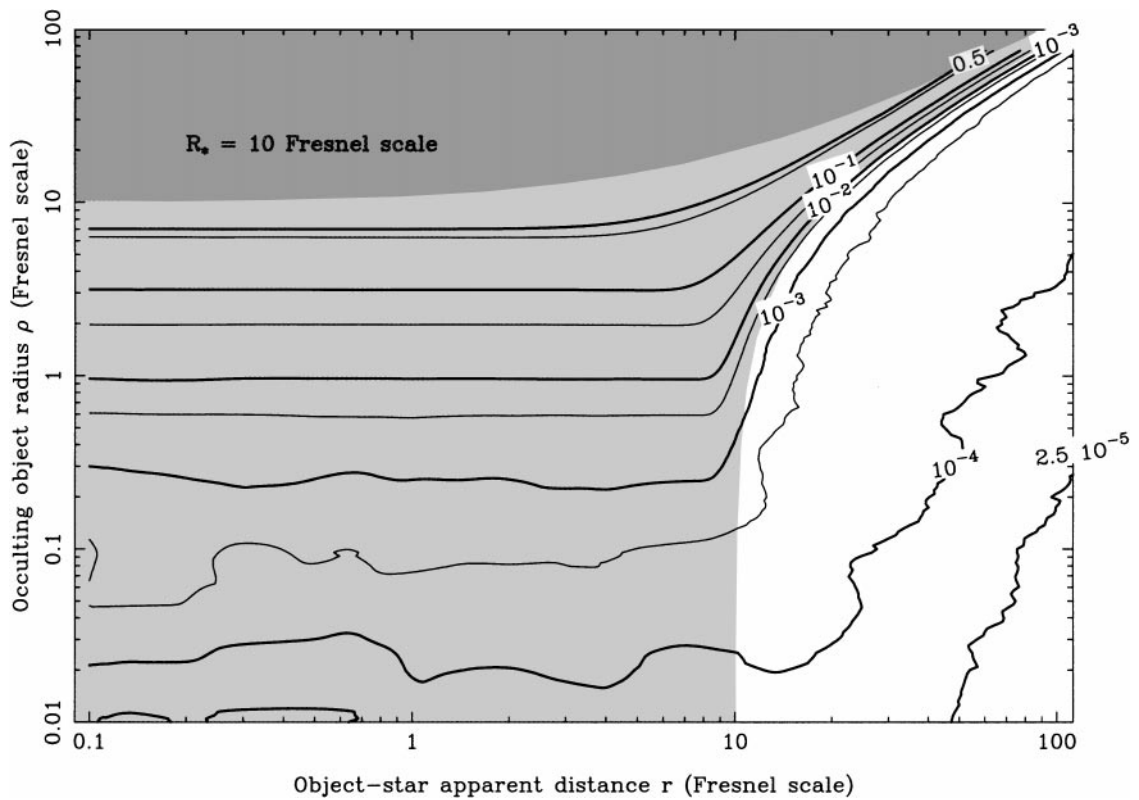
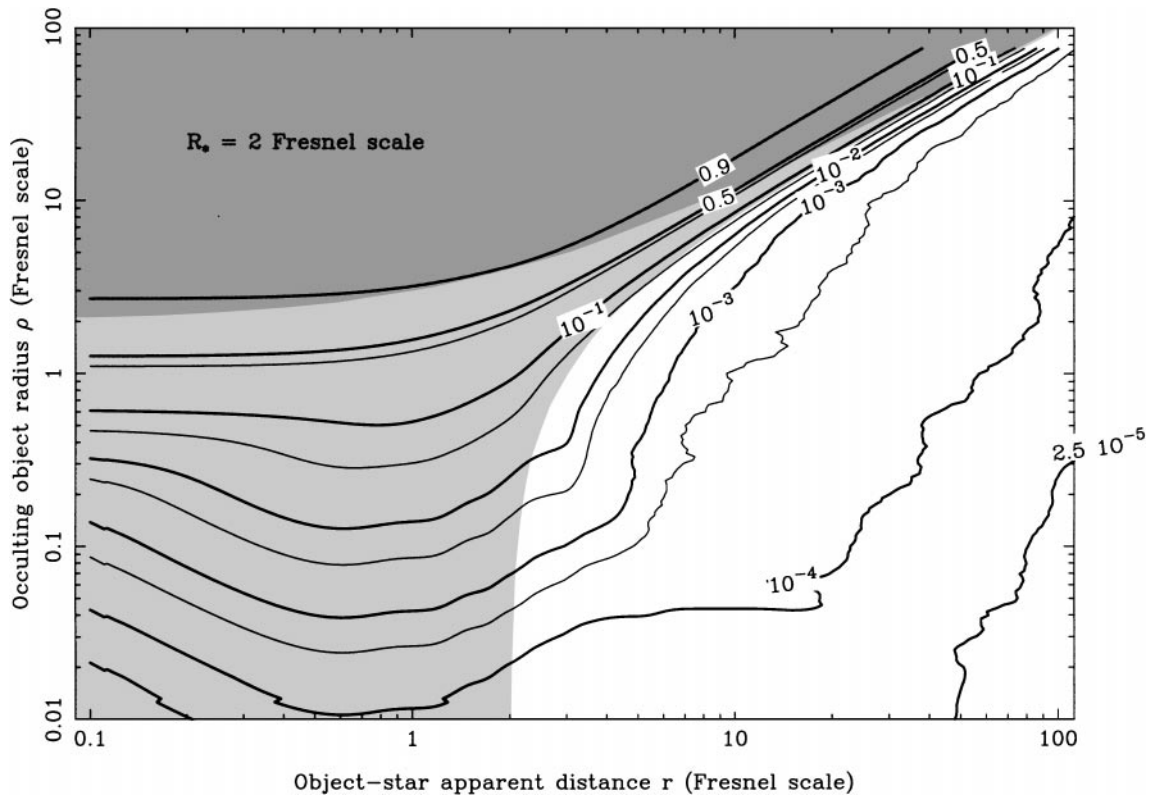


FIG. 3—Continued

TABLE I
Occultation Rate per Night (with the Minimum Size of Detectable KBO) as a Function of the Photometric Precision σ and the Stellar Radius R_* Projected at 40 AU (with Its Angular Radius Φ_*), for a Differential Size Distribution of KBOs Varying as ρ^{-4}

$R_*[\Phi_*]=$	0.1 km [0.003 mas]	0.5 km [0.017 mas]	1 km [0.034 mas]	2 km [0.07 mas]	10 km [0.34 mas]
$\sigma = 0.1$	0.01 (430 m)	0.006 (530 m)	0.004 (550 m)	8×10^{-4} (1.1 km)	3×10^{-5} (6.3 km)
$\sigma = 0.05$	0.06 (280 m)	0.03 (320 m)	0.01 (340 m)	0.003 (780 m)	8×10^{-5} (4.5 km)
$\sigma = 0.01$	2 (120 m)	0.5 (130 m)	0.2 (140 m)	0.05 (280 m)	1×10^{-3} (2 km)
$\sigma = 0.005$	6 (80 m)	1 (90 m)	0.6 (100 m)	0.2 (190 m)	0.003 (1.4 km)
$\sigma = 10^{-3}$	85 (40 m)	17 (40 m)	7 (45 m)	3 (80 m)	0.03 (630 m)
$\sigma = 5 \times 10^{-4}$	250 (25 m)	50 (30 m)	20 (30 m)	8 (55 m)	0.08 (450 m)

Note. All values computed from Eq. (14), with the detection threshold set to 4σ , the Fresnel scale set to 1 km, $v_o = 25$ km/s (opposition), $i = 0^\circ$, $H = 30^\circ$, and $\Delta t = 8$ h.

A constant slope for the differential size distribution and a radial distribution extending to 50 AU. The sensitivity of the occultation rates to the size distribution can be tested by considering another, less simple, model of the size distribution: The size distribution with a constant slope with $q = 4$ implies that KBOs smaller than 1 km radius have a collision time scale smaller than the age of the Solar System. Then, a more realistic model is a slope $q = 4$ for KBOs larger than 1 km radius and a smaller slope for smaller objects (B. J. Gladman, private communication). Observation of impact craters on Triton leads to a population of small objects in the outer Solar System governed by an index $q = 3$ for the differential size distribution (Stern and McKinnon 2000). This model reduces the number of occultations, as shown in Table II. For example, with a 0.1-km apparent star radius, the occultation rate is reduced by a factor 2 for $\sigma = 0.05$, by a factor 6 for $\sigma = 0.01$, and by a factor 20 for $\sigma = 5 \times 10^{-4}$.

Whatever the model we use, the radius ρ_{lim} of the smallest detectable object will be fixed by the observational parameters R_* , σ , and the Fresnel scale. So no information below this lower limit of detection can be obtained from such occultation observations. However, above this limit, since the occultation rate is very sensitive to the distribution slope, the method can provide strong constraints on the differential size distribution of the Kuiper belt population. We will return to this point in Section 5.2 since it actually depends on what and how the method is implemented.

TABLE II
Occultation Rate per Night Computed as in Table I but with a Differential Size Distribution Varying as ρ^{-3} for $\rho < 1$ km

$R_* =$	0.1 km	0.5 km	1 km	2 km	10 km
$\sigma = 0.1$	0.007	0.005	0.003	8×10^{-4}	3×10^{-5}
$\sigma = 0.05$	0.03	0.01	0.008	0.003	8×10^{-5}
$\sigma = 0.01$	0.3	0.1	0.06	0.02	10^{-3}
$\sigma = 0.005$	0.7	0.2	0.1	0.06	0.003
$\sigma = 10^{-3}$	5	1	0.7	0.3	0.02
$\sigma = 5 \times 10^{-4}$	11	3	1	0.7	0.05

Note. All other parameters set as in Table I.

5. HOW TO IMPLEMENT AND OPTIMIZE THE SEARCH FOR OCCULTATIONS BY KBOs

Our conclusion is thus that the search for occultations by KBOs using high-precision photometry is probably the only tool for exploring the small objects of the Kuiper belt. It is therefore important to discuss which observational parameters are necessary and/or possible to fit and what are the available facilities to implement and optimize such a method.

5.1. Optimizing the Apparent Stellar Size and the Apparent Velocity of KBOs

Let us first discuss what are the best stars for occultation by KBOs: as already said, the diameter of a typical star, projected at 40 AU, is between 0.1 and 100 km. As we saw in Section 3, the smaller the occulted star, the smaller the smallest detectable KBO, and because small KBOs are more numerous, the larger the occultation rates. The small stars will thus be good candidates to detect KBOs especially if they are bright enough to provide a good signal-to-noise ratio. For a given magnitude, the blue stars are smaller than the red ones (see Table III): an O5 star of $M_V = 12$ has a projected radius of 100 m. For the same magnitude, an M5 star has a projected radius of 10 km.

In addition to the apparent size of the star, a critical observational parameter is the data acquisition frequency. As seen in Section 2, the relative velocity v_o of the KBOs with respect to the star varies from a few to 25 km/s. Then the occultation length, which is roughly $\sim 2\rho_\epsilon/v_o$, is for most of them a fraction of a second. The quadrature direction can be exploited as proposed

TABLE III
Apparent Stellar Radii at 40 AU as a Function of the Spectral Class and Magnitude M_V

$M_V =$	8	10	12	14
M5 star	50 km	20 km	8 km	3 km
F5 star	4 km	2 km	700 m	100 m
O5 star	800 m	300 m	100 m	50 m

by Brown and Webster (1997) to search for occultations lasting several seconds. However, in this direction the occultation rate is lower than that toward the opposition since $N_{\text{occ}} \propto v_o$. So, if we use a photometer of sufficiently high speed, we will increase our chances of detecting KBOs by observing toward the opposition. Moreover, the frequency necessary to observe the diffraction fringes must be larger than $v_o/\sqrt{\lambda D/2}$. For visible wavelength, this minimum frequency varies from 1 to 20 Hz, which requires high-speed photometry.

5.2. Implementation Using High-Speed Photometry

High-speed photometric observations of stars have been developed to study rapidly evolving phenomena such as occultation by Solar System objects or asteroseismology. A complete analysis of the perturbations in a high-speed photometric lightcurve and in occultation lightcurves, in particular, can be found in Warner (1988). If the star is not too faint, the noise on a high time resolution lightcurve is dominated by scintillation which affects the stars independent of their brightness. The rms signal fluctuation observed with a telescope with a diameter d at an altitude h above the sea level can be written as (Young 1967)

$$\sigma = S_0 d^{-2/3} X^{3/2} e^{-h/H_0} (2\tau)^{-1/2}, \quad (15)$$

where X is the airmass, τ is the integration time, H_0 is taken to be 8 km, S_0 is a constant equal to 0.09 for conditions of good seeing, d is in centimeters, and τ is in seconds.

For $\tau = 1$ s, the rms fluctuations on a 2-m class telescope is roughly 3×10^{-3} under optimal conditions. According to Table I, this will allow us to detect (at 4σ) subkilometer objects. The largest ground-based telescopes (i.e., the 10-m class telescopes) allow us to marginally reach $\sigma \approx 10^{-3}$ and then to detect about 40-m radius KBOs (see Table I).

Some useful results, concerning the 2-, 4-, and 8-m class telescopes when observing O5 class stars for two magnitudes (12 or 10), are summarized in Fig. 4, where we have plotted the occultation rates per night as a function of the power law index q of the subkilometer KBO size distribution (with $q = 4$ for $\rho > 1$ km as in Table II). We have also indicated in this figure, for each telescope diameter, the approximate radius of the smallest detectable KBO. In each case, N_{occ} is computed for optimum observing conditions, i.e., O5 stars, observed from good sites, in the ecliptic and at the opposition, with telescopes equipped with a sufficiently rapid photometer (at least 20 Hz). Figure 4 shows that N_{occ} increases exponentially with q , but this variation also strongly depends on observational circumstances: We may thus expect that an observation campaign on various sites and/or with different instruments and/or observing different stars could

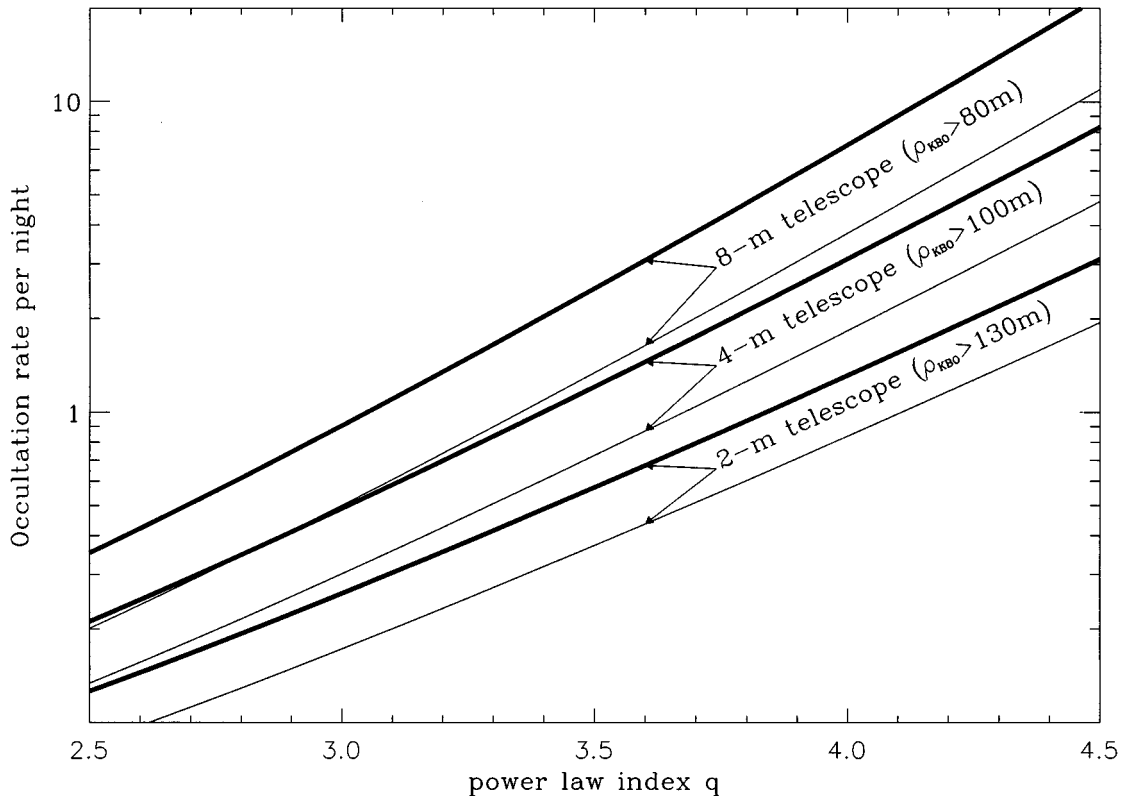


FIG. 4. Occultation rate per night as a function of the power law index q of the KBOs size distribution for 2-, 4-, and 8-m telescopes equipped with a 20-Hz photometer when observing an O5 star (under optimal conditions) of visual magnitude 12 (bold lines) or magnitude 10 (thin lines).

provide by cross-checking a good estimation of q concerning these elusive small KBOs. One can also see in Fig. 4 how important the choice of star is when implementing the search for occultations by KBOs: For example, the decrease in occultation rate is roughly the same when passing from an 8- to a 4-m telescope with an O5 star of 12th magnitude as when passing from a 12th to a 10th magnitude O5 star with an 8-m telescope.

Let us finally remark that, in Tables I and II, the $\sigma = 5 \times 10^{-4}$ case is unreachable from the ground, but might be achievable in space, if we obtain fast enough photometry on such space facilities (present or future). In this case, the number of occultations could indeed be spectacular and decisive for our knowledge of the Kuiper belt size distribution.

5.3. KBOs Research Using a CCD Camera

A possible approach for detecting KBOs by occultation is to observe several stars simultaneously for as long as possible. This requires the use of CCD cameras. The advantage of CCD cameras over photometers is that the probability of detection is multiplied by the number of stars; the limitation comes from the reduced acquisition frequency, which cannot, presently, be larger than a few hertz.

A program dedicated to the detection of KBOs has been developed in Taiwan, the Taiwan American Occultation Survey (TAOS) team, which deploys a set of small telescopes along a 7-km east–west baseline. These robotic 50-cm telescopes equipped with CCD cameras will automatically monitor 3000 stars. They expect to detect ten to thousands of events per year (see <http://www.taos.asiaa.sinica.edu.tw>).

Another possible tool for exploring the Kuiper belt is the space satellite COROT, a French mission of CNES dedicated to asteroseismology and studies of exoplanets by transit. To achieve this, COROT will perform high-precision photometric observation of several thousands of stars with a 25-cm telescope equipped with CCD cameras. The two fields, corresponding to the two programs, have slightly different optics. The two main programs will record continuously the same fields for six periods of five months, separated by one-month periods which can be used for complementary programs. The asteroseismology program will record a few very bright stars with an acquisition frequency of 1 Hz. The number of KBOs detected during this program will be limited by the large size and the small number of stars. With the above hypothesis concerning the KBO's size distribution, the detection rate will vary from one to one hundred per month, depending on the direction of observation. KBOs larger than 200 m can be detected. The extrasolar planets program will record thousands of stars. However, the minimum integration time will be 30 s. Hence the detection rate will be limited to 0.5 to 50 per month and the smallest detectable KBO will be 1 km. A program dedicated to the research of KBOs would record 100 stars with a frequency of 1 Hz and could detect 250 events per day. A one-month program could determine the spatial distribution and the size distribution of the objects (Roques 2000).

6. THE VALIDITY OF THE DETECTION

The main limitation of this method is the uniqueness of the occultation. It is not possible to redo an observation to verify the reality of the detection. Moreover, the objects detectable with this method are mostly undetectable by other techniques. Then the question is: How can we be sure we have detected an occultation by a KBO and not an asteroid, a comet, or a bird or an electric discharge?

This question has already been encountered during studies of planetary rings. The Uranus and the Neptune ring system, undetectable from the ground until recently, have been discovered and explored by stellar occultations. The reality of an occultation by the Uranus rings have been confirmed by the symmetrical dips observed on the two sides of the planet, but the incomplete arcs of Neptune have been much more difficult to catch. To assess the reality of an arc detection, the observations were conducted on two nearby telescopes. Some occultations provided arc profiles with S/N ratio good enough to fit the dip with a semitransparent bar model and reject the hypothesis of a solid body (Sicardy *et al.* 1991).

During planetary occultations, isolated events were often observed with one telescope but with S/N not good enough to fit them (Nicholson *et al.* 1990). One of them has been confirmed by simultaneous detection with nearby telescopes during an occultation by Uranus. It has been analyzed as the occultation by a 1.4-km object near Uranus (Sicardy *et al.* 1986). Using the present work, we found that the probability of occultation by KBOs during such observations was some tens of percent per night. Then, several isolated events observed during the planetary occultations could be due to KBOs.

Different methods can be used to assess the reality of the occultation and to possibly discriminate an occultation from a false event or an occultation by another object in the Solar System:

- As for planetary occultations, the reality of an occultation can be confirmed by simultaneous observation from nearby telescopes, or with multiobject photometers. However, this does not allow us to determine the distance of the occulting object.
- The direction of the shadow motion can also be used, as done by the TAOS team who validate the event by successive detections by telescopes spaced a few kilometers apart on an east–west baseline.
- Table IV shows the parameters of the occultations in terms of the distance of the occulting object. The minimum size of detectable objects (last column) shows that asteroids of a few tens of meters could be detected. However, the asteroid population is probably 10^5 times less numerous than the KBO population. Then, even if smaller objects are involved, the probability of occultation by KBOs is a thousand times larger than by asteroids.

The velocity of a KBO in the sky plane for a given direction depends on the distance of the occulting object (Eq. (5)). The probability of occultation is minimal and the duration of the occultation is maximal toward the quadrature, that is, 81°

TABLE IV

Occultation Parameters—Fresnel Scale F_{su} , Quadrature Direction ω , Apparent Velocity v_o at the Opposition, and Object Size Limit of Detectability ρ_{lim} —for Various Heliocentric Distances D_{AU} of the Occulting Object

D_{AU}	F_{su}^a	ω [quad.]	v_o [opp.]	ρ_{lim}^b
3.	245 m	55°	13 km/s	25 m
40.	1.1 km	81°	25 km/s	130 m
100.	1.7 km	84°	27 km/s	200 m
10^3	5.5 km	88°	29 km/s	700 m
10^4	17 km	89°	30 km/s	4 km
10^5	55 km	90°	30 km/s	55 km

^a At $0.4 \mu\text{m}$.

^b Detected at 4σ for $\sigma = 1\%$ and $\Phi_\star \sim 0.003$ mas.

from the opposition for objects at 40 AU from the Sun, but the direction of the quadrature changes with the distance of the occulting objects: When several events are detected, the number of events with respect to the direction of observation ω can be used to infer the distance of the population of occulting objects. The high occultation rates estimated above for large telescopes make these speculations plausible.

- If an occultation is observed at different wavelengths, the profiles are different (see Fig. 5), and the comparison of the dip

profiles could give information on the Fresnel scale and, then, on the distance of the occulting object.

- An occultation profile on a unique lightcurve with a high S/N and high-speed acquisition should exhibit the diffraction fringes (see Fig. 6 and Roques 2000). These features may be analyzed to retrieve the Fresnel scale and thus provide the distance of the occulting object (this analysis, like the previous point, is not in the scope of the present paper and will be carried out elsewhere).

7. SUMMARY AND FINAL REMARKS

In summary, here are the main points treated in the present paper:

- A model of the occultation phenomenon is derived taking diffraction into account: This diffraction greatly broadens the size of the KBO shadow (Section 3). The occultation rates computed with these diffracting models are much larger (Section 4) than those computed only using the geometric shadow (Section 2). We therefore expect the number of valid occultations (defined as a 4σ event) to increase from a few to several tens per night, if we obtain an rms signal fluctuation $\sigma \lesssim 1\%$ and observe stars in the ecliptic with angular radius $\lesssim 0.01$ mas.

- Occultation rates are computed for a differential size distribution $\propto \rho^{-q}$ with a constant index $q = 4$ (Table I); with a double

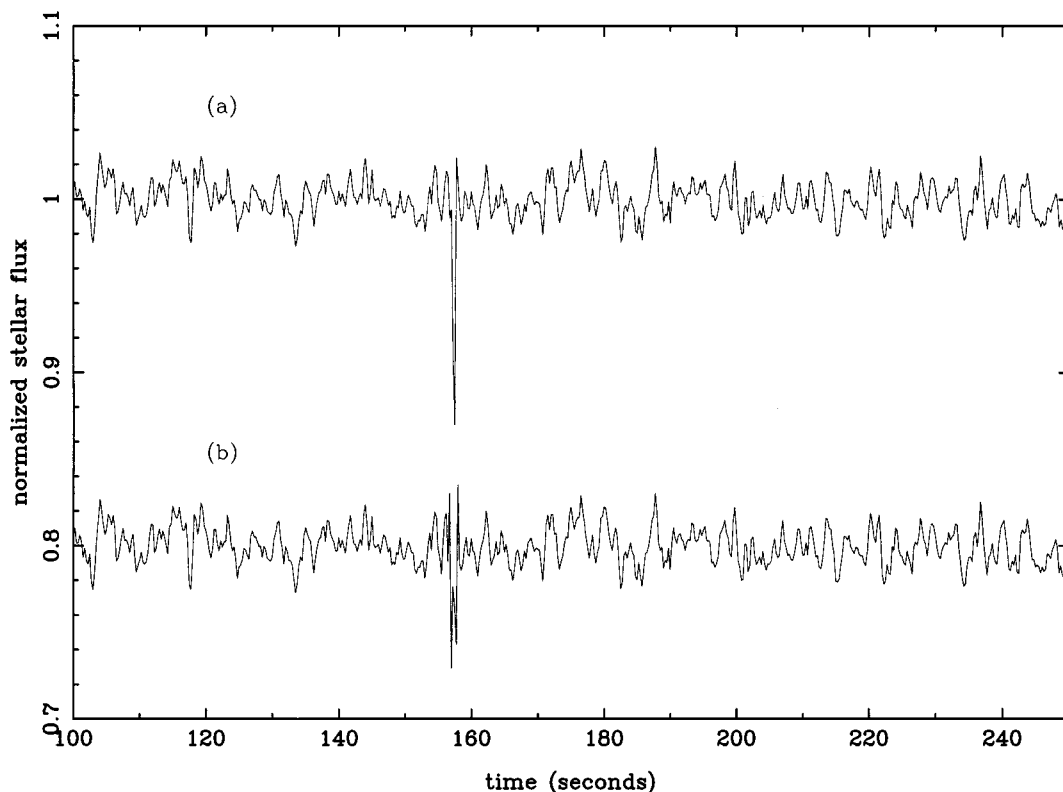


FIG. 5. Synthesized lightcurve of the occultation of a star by a 0.2-km KBO observed at $0.4 \mu\text{m}$ (upper curve) and $1.2 \mu\text{m}$ (lower curve). The star radius projected at 40 AU is 0.3 km and the noise $\sigma = 1\%$.

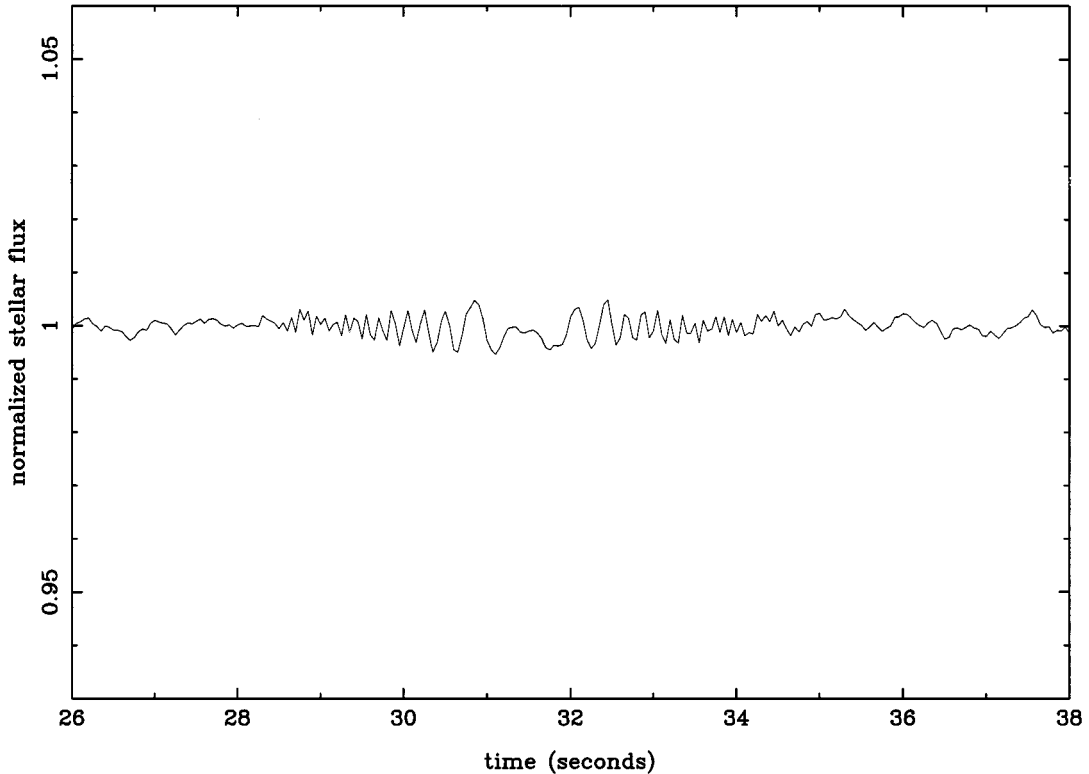


FIG. 6. Synthesized lightcurve of a stellar occultation observed with high photometric precision $\sigma = 0.001$ and exhibiting diffraction fringes. The object radius is 40 m and the star radius is 100 m, both projected at 40 AU. The acquisition frequency is 20 Hz and the object apparent velocity is 3 km/s.

index differential size distribution, $q = 4$ for objects larger than 1 km, and for subkilometer objects, q varies from 2.5 to 4.5 (Fig. 4). The differences between the occultation rates for different sites, instruments, or occulted stars show that, with several occultation data sets, it should be possible to provide a good estimation of q for the small KBOs.

—The main limitation of the photometric precision comes from the scintillation of the star, which remains about the same to a visual magnitude of ~ 12 . The blue O5 stars are the best candidates for detecting KBOs since they have the smallest angular radius (~ 100 m at 40 AU) for 12th magnitude.

—Stellar occultations by Solar System small objects involve very rapid fluctuations of the stellar flux ($\gtrsim 1$ Hz), so that rapid photometry must be used. Moreover, the occultation events are shorter but more numerous when observed in the antisolar direction, so we may optimize the detections of KBOs with a high-speed photometer ($\gtrsim 20$ Hz).

—In the near future, observations with the French space mission COROT will provide an excellent opportunity to explore the Kuiper belt using this occultation research method.

We have shown here that stellar occultations can detect a population of very small objects, invisible by other observation methods, and that these detections can be statistically exploited if the population has a sufficient surface density on the sky. In

particular this is the only method for detecting the population of small (subkilometer-sized) KBOs which should contain most of the mass of the Kuiper belt. Let us note however that such an observation of serendipitous occultations is not a discovery of each occulting object because the orbit of the object remains unknown. In other words, this method allows us to explore the population as a whole, but not the individual objects.

We foresee two ways to extend the present work: On one hand, the simultaneous observation of an occultation at two different wavelengths provides events of different depth, which could allow us to retrieve the Fresnel scale and then to determine the distance of the occulting object. On the other hand, if we could obtain both high-speed and high-precision photometric observations (on a telescope > 5 m or from space), we could observe the diffraction fringes of each occultation event and identify individually, instead of statistically, the occulting objects. In this case, we could deduce the object size and location by fitting our occultation model to the precise light profile of the event. Then occultation could also be used to explore other small body populations in the Solar System, *a priori* more rare in the sky than the KBOs, such as asteroids or comets in the Oort clouds, or small bodies possibly confined as a nest of gravitational stability, as the Lagrangian points of the planets. It is currently very difficult to evaluate the probability of observing occultations by such objects but we think these points deserve further investigation.

REFERENCES

- Bailey, M. E. 1976. Can invisible bodies be observed in the Solar System? *Nature* **259**, 290–291.
- Born, M., and E. Wolf 1980. Elements of the theory of diffraction. In *Principles of Optics* (6th ed.), pp. 370–458. Pergamon Press, New York.
- Brown, M., and R. Webster 1997. Occultation by Kuiper belt Objects. *Mon. Not. R. Astron. Soc.* **289**, 783–786.
- Dyson, F. J. 1992. Hunting for comets and planets. *Quart. J. R. Astron. Soc.* **33**, 45–57.
- Elliot, J. L., and C. B. Olkin 1996. Probing planetary atmospheres with stellar occultations. *Annu. Rev. Earth Planet. Sci.* **24**, 89–123.
- Jewitt, D. 1999. Kuiper belt objects. *Ann. Rev. Earth Planet. Sci.* **27**, 287–312.
- Jewitt, D., and J. Luu 1995. The Solar System beyond Neptune. *Astron. J.* **109**, 1867–1876.
- Kuiper, G. 1951. On the origin of the Solar System. In *Astrophysics: A Topical Symposium* (J. A. Hynek, Ed.), pp. 357–424. Mc Graw–Hill, New York.
- Luu, J., and D. Jewitt 1998. Deep imaging of the Kuiper belt with the Keck 10-meter telescope. *Astrophys. J.* **502**, L91.
- Nicholon, P. D., M. L. Cooke, K. Matthews, J. H. Elias, and G. Gilmore 1990. Five stellar occultations by Neptune: Further observations of ring arcs? *Icarus* **87**, 1–39.
- Rabinowitz, D., E. Bowell, E. Schoemaker, and K. Muinonen 1994. The population of Earth-crossing asteroids. In *Hazard Due to Comets and Asteroids* (T. Gehrels, Ed.), pp. 285–306. Univ. of Arizona Press, Tucson.
- Roques, F. 2000. Detection of the small EKB objects by occultation. In *MBOSS ESO workshop proceeding*. ESO Springer conferences series, in press.
- Roques, F., M. Moncuquet, and B. Sicardy 1987. Stellar occultations by small bodies: Diffraction effects. *Astron. J.* **93**, 1549–1558.
- Schneider, G., B. A. Smith, E. E. Becklin, D. W. Koerner, R. Meier, D. C. Hines, P. J. Lowrance, R. J. Terrile, R. I. Thompson, and M. Rieke 1999. NICMOS imaging of the HR 4796A circumstellar disk. *Astrophys. J.* **513**, L127–L130.
- Sicardy, B., F. Roques, A. Brahic, P. Bouchet, J. P. Maillard, and C. Perrier 1986. More dark matter around Uranus and Neptune? *Nature* **320**, 729–731.
- Sicardy, B., F. Roques, and A. Brahic 1991. Neptune's rings, 1983–1989: Ground-based stellar occultation observations. *Icarus* **89**, 220–243.
- Stern, A., and W. B. McKinnon 2000. Triton's surface age and impactor population revisited in light of Kuiper belt fluxes: Evidence for small Kuiper belt objects and recent geological activity. *Astron. J.* **119**, 945–952.
- Stone, R. C., S. W. McDonald, and J. L. Elliot 1999. 5145 Pholus stellar occultation candidates 1999–2005. *Astron. J.* **118**, 591–599.
- Warner, B. 1988. *High Speed Astronomical Photometry*. Cambridge Astrophysics Series, Cambridge Univ. Press, Cambridge.
- Young, A. T. 1967. Photometric error analysis VI. Confirmation of Reiger's theory of scintillation. *Astron. J.* **72**, 747–753.